Supporting Information

Strong deformation of ferrofluid-filled elastic alginate capsules in inhomogenous magnetic fields

Christian Wischnewski,[†] Elena Zwar,[‡] Heinz Rehage,[‡] and Jan Kierfeld[*,†]

†*Department of Physics, Technische Universität Dortmund, 44221 Dortmund, Germany*
‡*Department of Chemistry, Technische Universität Dortmund, 44221 Dortmund, Germany*

E-mail: jan.kierfeld@tu-dortmund.de

8 pages, 6 figures, 1 table

Shape equations

In order to calculate axisymmetric shapes of capsules under the influence of external magnetic forces we numerically solve a closed set of six shape equations, which are based on non-linear Hookean elasticity of the material. We recapitulate the shape equations in this section briefly. For more details on the elastic model and the derivation of the shape equations, see Refs. S1,S2 and Ref. S3 in the presence of magnetic forces.

The capsules' shells are thin enough to be effectively treated as two-dimensional. We parametrize the surface in cylindrical coordinates (r, z, φ) (see Figure S1). Because of rotational symmetry, the contour line of the capsule can be written as $z(r)$. The arc length s of the contour line starts at the lower apex with $s = 0$ und ends at the upper apex with $s = L$.

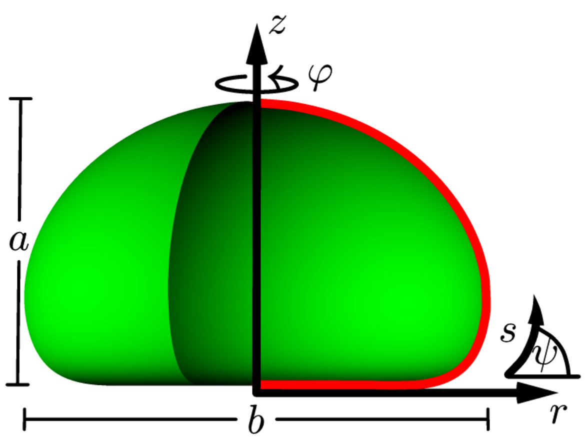

Figure S1: Parametrization of the axisymmetric capsule surface in cylindrical coordinates. The red contour line is calculated numerically.

We use a Hookean elastic energy density

$$\begin{aligned} w_S = &\frac{1}{2}\frac{Y_{2\mathrm{D}}}{1-\nu^2}(e_s^2 + 2\nu e_s e_\varphi + e_\varphi^2) \\ &+\frac{1}{2}E_\mathrm{B}(K_s^2 + 2\nu K_s K_\varphi + K_\varphi^2). \end{aligned} \tag{S1}$$

The strains e_i are related to the stretch factors λ_i via $e_i = \lambda_i - 1$ and the bending strains K_i are related to the curvatures κ_i via $K_i = \lambda_i\kappa_i - \kappa_{i_0}$. The index s describes the meridional direction and φ the circumferential direction. The index 0 indicates the reference sphere. The bending modulus E_B is defined via

$$E_\mathrm{B} = \frac{Y_{2\mathrm{D}}h^3}{12(1-\nu^2)}. \tag{S2}$$

The constitutive relations

$$\tau_s = \frac{Y_{2\mathrm{D}}}{1-\nu^2}\frac{1}{\lambda_\varphi}(e_s + \nu e_\varphi), \tag{S3}$$

$$m_s = E_\mathrm{B}\frac{1}{\lambda_\varphi}(K_s + \nu K_\varphi) \tag{S4}$$

for the ealstic stresses τ_i and the bending moments m_i (τ_φ and m_φ with interchanged indices) are obtained by variation of the energy density with respect to the strains.

The shape equations follow from purely geometric relations and the force and moment equilibrium in the shell, which is described by the following three equations (normal and tangential force equilibrium and moment equilibrium):

$$\begin{aligned} 0 = &(\tau_s + \gamma)\kappa_s + (\tau_\varphi + \gamma)\kappa_\varphi \\ &- (p_0 \Delta\rho g z + f_m) + \frac{1}{r}\frac{\mathrm{d}(rq)}{\mathrm{d}s}, \end{aligned} \tag{S5}$$

$$0 = \frac{\cos\psi}{r}\tau_\varphi + \kappa_s q - \frac{1}{r}\frac{\mathrm{d}(r\tau_s)}{\mathrm{d}s}, \tag{S6}$$

$$0 = q + \frac{1}{r}\frac{\mathrm{d}(rm_s)}{\mathrm{d}s} - \frac{\cos\psi}{r}m_\varphi. \tag{S7}$$

Rearranging these equilibrium equations and geometrical relations for r, z and ψ, we get a system of six differential equations, the shape equations:

$$r'(s_0) = \lambda_s \cos\psi, \tag{S8}$$

$$z'(s_0) = \lambda_s \sin\psi, \tag{S9}$$

$$\psi'(s_0) = \lambda_s \kappa_s, \tag{S10}$$

$$\tau_s'(s_0) = \lambda_s\left(\frac{\tau_\varphi - \tau_s}{r}\cos\psi + \kappa_s q - p_s\right), \tag{S11}$$

$$m_s'(s_0) = \lambda_s\left(\frac{m_\varphi - m_s}{r}\cos\psi - q\right), \tag{S12}$$

$$\begin{aligned} q'(s_0) = \lambda_s\Big(&- \kappa_s(\tau_s + \gamma) - \kappa_\varphi(\tau_\varphi + \gamma) \\ &- \frac{q}{r}\cos\psi + p_0 + \Delta\rho g z + f_m\Big). \end{aligned} \tag{S13}$$

The first three equations are geometrical relations, while the remaining three equations represent force and moment equilibrium. The pressure p_0 inside the capsule is modified by the hydrostatic pressure $\Delta\rho g z$ and the magnetic pressure f_m. This system is closed by the following relations:

$$\lambda_s = (1-\nu^2)\lambda_\varphi \frac{\tau_s}{Y_{2D}} - \nu(\lambda_\varphi - 1) + 1, \tag{S14}$$

$$\lambda_\varphi = \frac{r}{r_0}, \tag{S15}$$

$$K_s = \frac{1}{E_B}\lambda_\varphi m_s - \nu K_\varphi, \tag{S16}$$

$$K_\varphi = \frac{\sin\psi - \sin\psi_0}{r_0}, \tag{S17}$$

$$\kappa_s = \frac{K_s + \kappa_{s_0}}{\lambda_s}, \tag{S18}$$

$$\kappa_\varphi = \frac{\sin\psi}{r}, \tag{S19}$$

$$\tau_\varphi = \frac{Y_{2D}}{1-\nu^2}\frac{1}{\lambda_s}((\lambda_\varphi - 1) + \nu(\lambda_s - 1)), \tag{S20}$$

$$m_\varphi = \frac{E_B}{\lambda_s}(K_\varphi + \nu K_s) \tag{S21}$$

We solve the closed system of six shape equations numerically with a fourth order Runge-Kutta scheme. Boundary conditions at the two poles follow from the requirement of a closed capsule and lead to a boundary value problem that is solved by employing a multiple shooting method in conjunction with the Runge-Kutta scheme.

Analysis of elastic parameters

For the spinning capsule experiments, we used the SVT 20 of the DataPhysics Instruments GmbH. We used Fluorinert 70 (FC 70) as outer phase because of its high density. The initial undeformed (quiescent) state was recorded at 2000 rpm. In Figure S2, a sketch of the spinning capsule measurement technique is shown.

Capsule compression experiments were performed with the DCAT11 tensiometer (DataPhysics Instruments GmbH) with the respective software SCAT. The compression speed was set to 0.02 mm/s. A sketch of the capsule compression method is shown in Figure S3.

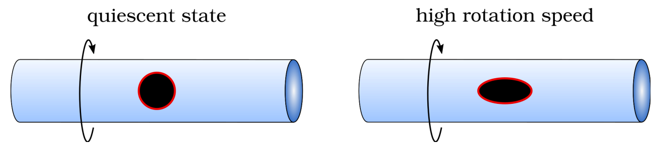

Figure S2: Spinning capsule experiment.

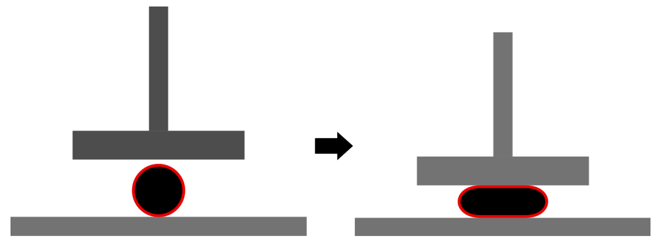

Figure S3: Capsule compression experiment.

Measurement of initial radius R_0 and volume V_0 of capsules

The radius R_0 of the initial undeformed spheres can not be measured directly, because the capsules are deformed by gravity even without an external magnetic field. Therefore, we determine the capsules' volume from the experimental images. The image analysis was performed with FIJI/ImageJ[S4,S5]) using capsule photos taken with a OCA20 pendant drop tensiometer (DataPhysics Instruments GmbH).

In order to determine the volume V_0, we measure the axial radius r_i at different heights z_i and calculate $V_0 = \int dz \pi r^2(z) \approx \sum_i \pi r_i^2 (z_{i+1} - z_i)$ by summation over small cylindrical volumes of radius r_i at height z_i. We then calculate the initial radius by $R_0 = (3/(4\pi)V_0)^{(1/3)}$. We only assume that capsules are axisymmetric, which is fulfilled to a good approximation.

We find that the volume inside the capsule is constant during the whole experiment. The elastic shell is impermeable for the involved fluids.

Scanning electron microscopy (SEM) images

In order to estimate the shell thickness, SEM measurements were performed. The resulting images are shown in Figure S4. The capsule was broken prior to the measurement to avoid bursting in ultra high vacuum.

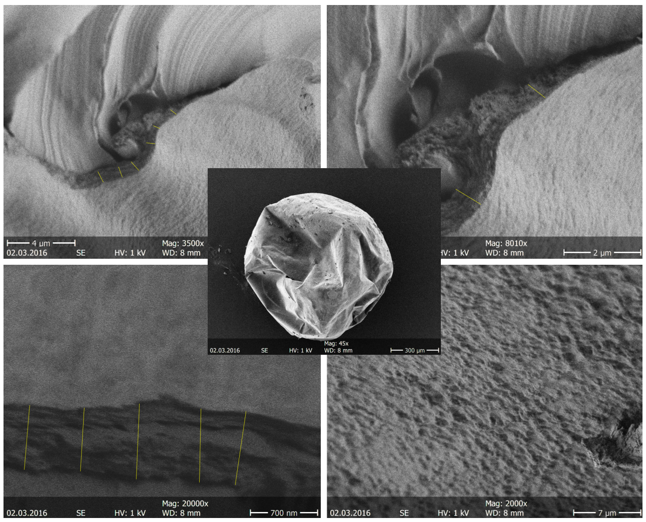

Figure S4: Scanning electron microscopy images of the ferrofluid-filled capsules. Center: complete capsule, bottom right: outer capsule shell. Top left, top right and bottom left: cross sections through ruptured parts of the shell at increasing megnification; yellow lines measure shell thickness.

This gives only a rough estimate of the thickness of the capsule shell. In addition to potential errors due to optical effects like parallax error it has to be taken into account that SEM is performed in vacuum, i.e., in the dried unhydrated state. With our optical microscope we were not able to resolve the hydrated shell of intact capsules, from which we can conclude that the shell thickness of the hydrated capsules has to be below 5 μm. From the SEM images we find a shell thickness of approximately 600 nm in vacuum in the dried state, see yellow lines in Figure S4. For alginate capsules with thicker shells we could perform both optical microscopy measurements in the hydrated state and SEM measurements in the dried state. These measurements suggest swelling factors larger than 5 for the thickness increase by hydration. We conclude that the shell thickness in the hydrated state is approximately 3 μm with a relatively high error around 1 μm.

Fit of the external magnetic field

The external magnetic field generated by a coil with a conical iron core was measured with a hall probe. The field was measured on different positions on the central axis over the iron core and in the vicinity of the axis.

We found that the field was nearly constant in radial direction within a distance of about 2 mm next to the central axis. Our biggest capsule had a radius of $R_0 = 1.044$ mm and even in the deformed state, its radial dimension did not exceed 1.4 mm. So it is well justified to treat the magnetic field as constant in radial (r-) direction and to set the radial component of the field B_r to zero. Together with the cylindrical symmetry of the setup, we only have to estimate the z-component B_z that depends on the coordinate z and the current I. We use a Langevin function to model the current dependency and a hylerbolic function for the position dependency. The measured magnetic field is in good agreement with a fit

$$B_z(z, I) = a\left(\coth(b_I I) - \frac{1}{b_I I}\right)\left(\frac{a_z}{z - b_z} + c_z\right) \tag{S22}$$

with parameters

$$a = 4.647 \tag{S23}$$

$$b_I = 0.332\,\frac{1}{\mathrm{A}} \tag{S24}$$

$$a_z = 286.7 \cdot 10^{-6}\,\mathrm{Tm} \tag{S25}$$

$$b_z = -1.104 \cdot 10^{-3}\,\mathrm{m} \tag{S26}$$

$$c_z = 10.86 \cdot 10^{-3}\,\mathrm{T}. \tag{S27}$$

The fit describes the magnetic field with an error below 1 % in the neighborhood of the capsule. A plot of the z- and I-dependence of the B_z is shown in Figure S5.

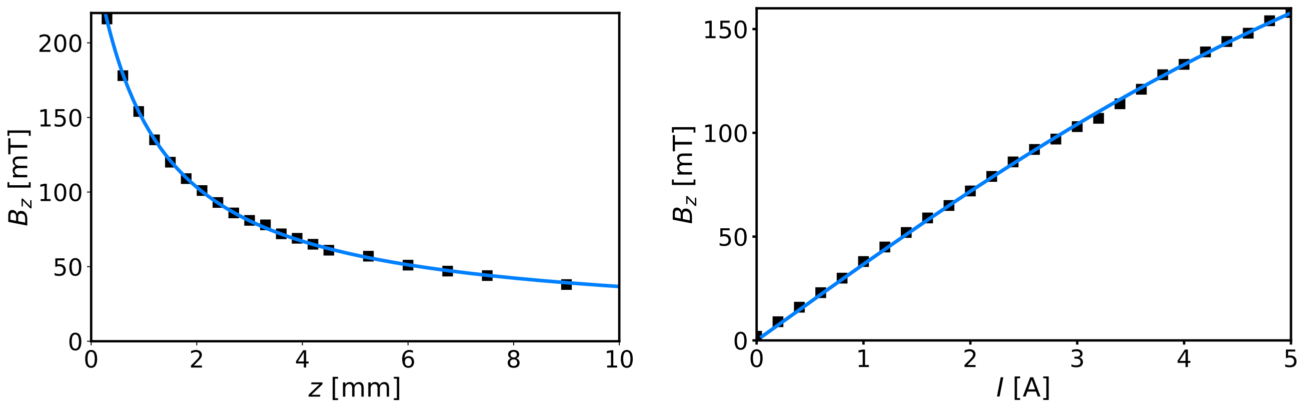

Figure S5: Magnetic flux density B_z in z-direction as a function of the vertical distance z to the iron core for $I = 2\,\text{A}$ (left) and as a function of the current I in the coil for $z = 3.6\,\text{mm}$ (right). The fit eq S22 is shown as solid lines.

Dynamic light scattering

To ensure the stability of the nanoparticles inside the ferrofluid dynamic light scattering measurements were performed. We used the Zeta-Sizer Nano ZS by Malvern instruments with the Zetasizer Software 7.12. The results were analysed with the CONTIN fit. All particle size values are given as the so-called *number mean*.

The capsules were produced by formation in a layer of distilled water followed by sinking into layer of aqueous sodium alginate solution (1‰_w). The polymerisation time needed for the formation of stable, ferrofluid-filled capsules was 30 s. The procedure is shown in Figure 1 in the main text.

Additional interface tension in capsule compression experiments

The original Reissner formula

$$F = \frac{4Y_{2\text{D}}h}{R_0\sqrt{3(1-\nu^2)}}\,d \tag{S28}$$

for the force-displacement relation describes the linear response of an unpressurized and initially tension-free elastic shell with rest radius R_0 to a point force F in terms of the resulting indentation d. In the presence of an additional interfacial tension, the main difference to the purely elastic shell is a non-vanishing pressure p_0, which is caused by the interfacial tension already in the initial state with $F = 0$ and which satisfies the Laplace-Young equation

$$2\gamma/R_0 = p_0. \tag{S29}$$

We generalize Reissner's linearized shallow shell theory[S6,S7] to include the interfacial tension and the resulting internal pressure p_0 (in Ref. S8 the related problem of pressurized shells in the absence of an interfacial tension has been considered). This leads to a linearized shallow shell equation

$$\kappa_B\nabla^4 w - \gamma\nabla^2 w + \frac{Y_{2\text{D}}}{R_0^2}w = -\frac{F}{2\pi}\frac{\delta(r)}{r} \tag{S30}$$

for the normal displacement $w(r)$ in polar coordinates, with r as the radial distance from the origin where the point force F is applied; κ_B is the shell's bending modulus

$$\kappa_B = \frac{Y_{2\text{D}}h^2}{12(1-\nu^2)}. \tag{S31}$$

Equation (S30) is identical to the linearized shallow shell equation governing the indentation of pressurized shells with internal pressure p_0 in the absence of interfacial tension (eq (3.2) in Ref. S8) with the interfacial tension $\gamma = p_0R_0/2$ (according to Laplace-Young equation S29) replacing the pressure-induced isotropic stress $\sigma_\infty = p_0R_0/2$. This means both problems are equivalent: the interfacial tension gives rise to an internal pressure p_0 in the same way as an internal pressure p_0 gives rise to an isotropic tension σ_∞ prior to indentation. Consequently the solution of eq (S30) proceeds as in Ref. S8. Integrating eq (S30) The solution $w(r)$ for a given indentation $d = -w(0)$ has to be integrated over the whole reference plane of shallow shell theory to obtain the force $F = -2\pi(Y_{2D}/R_0^2)\int_0^\infty dr r w(r)$. This finally gives

$$F = \frac{4Y_{2D}h}{R_0\sqrt{3(1-\nu^2)}}\,G(\tau)\,d \tag{S32}$$

with

$$G(\tau) = \frac{\pi}{2}\frac{(\tau^2-1)^{1/2}}{\operatorname{artanh}(1-\tau^{-2})^{1/2}} \tag{S33}$$
$$\tau = 3(1-\nu^2)\,(\gamma/Y_{2D})^2\,(R_0/h)^2\,.$$

For $\gamma \approx 0$ the Reissner result (S28) is recovered (note that in this case $\tau \approx 0$ and both the numerator and the denominator in (S33) become imaginary because $0 < \tau < 1$). For finite $\gamma > 0$ we find a stiffening of the shell, i.e., an increased linear stiffness F/d as in Ref. S8 for pressurized shells ($G(\tau) > 1$ for $\tau > 0$). The increase in linear stiffness remains small for $\tau \ll 1$ ($G(\tau) \approx 1$ for $\tau \ll 1$), which is fulfilled for capsule materials with ν sufficiently close to unity as for our alginate capsules. Therefore, corrections due to $\gamma > 0$ remain small.

Additional interface tension in spinning drop experiments

We also have to generalize the analysis of capsule deformation in the spinning drop apparatus given in Ref. S9 in the presence of interfacial tension. The linear response of the capsule deformation in spinning drop experiments is actually equivalent to the deformation of a ferrofluid-filled capsule in a small uniform external magnetic field as it has been analyzed in Ref. S3 if we set the magnetic susceptibility to $\chi = -1$ and the magnetic field strength to $\mu_0 H^2 = \Delta\rho R_0^2\omega^2$. Both magnetic forces on the ferrofluid-filled capsule in an external field and the centrifugal pressure exerted by a liquid of different density inside the capsule are normal forces (as they are generated by liquids) acting on the capsule surface. For a spherical shape the magnetic normal forces have the same position-dependence on the polar angle (between the radial vector and the symmetry axis, i.e., field or rotation axis) for a susceptibility $\chi = -1$; for $\mu_0 H^2 = \Delta\rho R_0^2\omega^2$ also the magnitude of magnetic and centrifugal forces becomes identical. In Ref. S3 the deformation of a ferrofluid-filled magnetic capsule has already been considered also in the presence of an interfacial tension γ, and we can simply adapt the results for the linear response, which are derived in Appendix A of Ref. S3, to the capsule deformation in the spinning drop apparatus by exploiting the equivalence of both problems.

For completeness we repeat the major steps of the calculation. The linear response theory is of first order in the displacements $(u_r, u_\varphi, u_\theta)$ in spherical coordinates with the polar angle θ and the azimuthal angle φ and $\theta = 0$ as the rotation axis (note that in Ref. S9 the notation is different: the azimuthal angle is denoted by θ and the polar angle by ϕ). In the elastic shell, the equilibrium of forces has to be fulfilled in tangential and normal direction. The tangential force equilibrium is given as

$$\frac{\mathrm{d}}{\mathrm{d}\theta}(R_0\tau_\theta\sin\theta) = R_0\tau_\varphi\cos\theta$$

and the normal equilibrium as

$$\frac{1}{R_0}(\tau_\theta+\tau_\varphi) + (\kappa_\theta+\kappa_\varphi)\gamma = p_0 + \frac{1}{2}\Delta\rho R_0^2\omega^2\sin^2\theta.$$

The curvatures κ_φ and κ_θ are expanded to first order in the displacements via

$$\kappa_\theta+\kappa_\varphi \approx \frac{2}{R_0} - \frac{1}{R_0^2}(2u_r - \partial_\theta^2 u_r + \partial_\theta u_r\cot\theta).$$

The coupled equation system describing force balance has to be solved using the constitutive relations

$$\tau_\varphi - \nu\tau\theta = \frac{Y_{2D}}{R_0}(u_\theta \cot\theta + u_r)$$
$$\tau_\theta - \nu\tau\varphi = \frac{Y_{2D}}{R_0}(\partial_\theta + u_r)$$

and the boundary conditions $\partial_\theta u_r(0) = \partial_\theta u_r(\pi/2) = 0$ and $u_\theta(0) = u_\theta(\pi/2) = 0$. The ansatz

$$u_r = A + B\cos^2\theta$$
$$u_\theta = C\sin\theta\cos\theta,$$

describes a spheroidal shape, preservation of volume requires $A = -B/3$. Using this spheroidal ansatz we find the solution

$$A = \frac{\Delta\rho R_0^4\omega^2(5+\nu)}{24[Y_{2D} + (5+\nu)\gamma]}$$
$$B = -3A$$
$$C = \frac{\Delta\rho R_0^4\omega^2(1+\nu)}{4[Y_{2D} + (5+\nu)\gamma]}.$$

To calculate the deformation parameter D, we use $r(\theta) = R_0 + u_r$ and find

$$D = \frac{r(0) - r(\pi/2)}{r(0) + r(\pi/2)} \approx \frac{B}{2R_0} = \frac{-\Delta\rho R_0^4\omega^2(5+\nu)}{16[Y_{2D} + (5+\nu)\gamma]}. \quad \text{(S34)}$$

For $\gamma \approx 0$ we recover the well-known result from Ref. S9,

$$D = -\Delta\rho\omega^2 R_0^3 \frac{(5+\nu)}{16Y_{2D}}, \quad \text{(S35)}$$

This means that, in the presence of an interfacial tension $\gamma > 0$, we simply have to replace Y_{2D} in eq S35 by $Y_{2D} + (5+\nu)\gamma$ resulting in a reduction of the deformation D. Analyzing the same experimental spinning capsule deformation data should give identical values of $Y_{2D} + (5+\nu)\gamma$. Analyzing the same data assuming $\gamma > 0$ will thus reduce the inferred result for the Young's modulus by $(5+\nu)\gamma$.

Including an interfacial tension γ into the combined analysis of spinning drop and capsule compression experimental data thus results in a reduced elastic modulus $Y_{2D} \to Y_{2D} - (5+\nu)\gamma$ to fit the spinning drop data with eq (S34). If $\gamma/Y_{2D} \ll 1$ such that $\tau \ll 1$ in eq (S32), ν is increased at the same time such that $Y_{2D}/\sqrt{1-\nu^2}$ remains approximately unchanged to fit the capsule compression data with eq (S32).

Sensitivity of the capsule deformation to the Poisson number ν

A Poisson ratio close to unity gives rise to a large area compression modulus $K_{2D} = Y_{2D}/2(1-\nu)$, which becomes sensitive to changes in ν and, thus, also large elastic stresses, which contain factors $1/(1-\nu)$ and become very sensitive to changes in ν (see prefactors $1/(1-\nu^2)$ in the elastic stresses in eq S20. Small deviations in ν lead to considerable changes in τ_i and visibly changing shapes of the capsule. Figure S6 shows simulations of capsule 1 with five slightly different Poisson ratios ranging from $\nu = 0.926$ to $\nu = 0.966$. While there are only minor deviations in the weakly deformed state in the absence of magnetic fields ($I = 0\,\mathrm{A}$), where the capsule is only deformed by gravity and tensions are dominated by the ν-independent interface tension, the capsule's side ratio a/b shows obvious differences in the strongly deformed state ($I = 5\,\mathrm{A}$), which is dominated by large elastic tensions. In conclusion, strongly deformed shapes are better suited to determine the value of ν. We can estimate the error of the numerically determined value of ν to be smaller than 0.01.

List of chemicals

All chemicals including purity are shown in table S1. All chemicals were used without further purification.

References

[S1] Knoche, S.; Kierfeld, J. Buckling of spherical capsules. *Phys. Rev. E* **2011**, *84*,

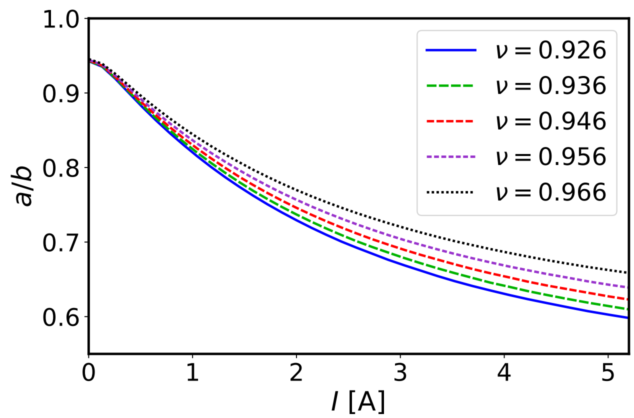

Figure S6: Ratio of the height a to width b of capsule 1 for increasing current I with $\nu = 0.926, 0.936, 0, 946, 0.956, 0.966$.

Table S1: List of chemicals

Chemical	Manufacturer	Quality
Calcium chloride anhyd.	Merck	98%
Chloroform	Merck	p. A.
Diphenyl ether	Acros Organics	99%
Ethanol	VWR	99,5%
Fluorinert (FC-70)	abcr	-
n-Hexane	Merck	$\geq$96%
1-Hexanol	Merck	$\geq$ 98%
1,2-Hexadecanediol	Sigma Aldrich	90%
Iron acetyl acetonate	Alfa Aesar	-
Oleic acid	VWR	81%
Oleylamine	Sigma Aldrich	70%
Sodium alginata	Aldrich	-
Sodium chloride	VWR	-

046608.

[S2] Knoche, S.; Kierfeld, J. The secondary buckling transition: Wrinkling of buckled spherical shells. *Eur. Phys. J. E* **2014**, *37*, 62.

[S3] Wischnewski, C.; Kierfeld, J. Spheroidal and conical shapes of ferrofluid-filled capsules in magnetic fields. *Phys. Rev. Fluids* **2018**, *3*, 043603.

[S4] Schindelin, J. et al. Fiji: an open-source platform for biological-image analysis. *Nature Methods* **2012**, *9*, 676–682.

[S5] Rueden, C. T.; Schindelin, J.; Hiner, M. C.; DeZonia, B. E.; Walter, A. E.; Arena, E. T.; Eliceiri, K. W. ImageJ2: ImageJ for the next generation of scientific image data. *BMC Bioinformatics* **2017**, *18*, 529.

[S6] Reissner, E. Stresses and Small Displacements of Shallow Spherical Shells. I. *J. Math. Phys.* **1946**, *25*, 80.

[S7] Reissner, E. Stresses and Small Displacements of Shallow Spherical Shells. II. *J. Math. Phys.* **1946**, *25*, 279–300.

[S8] Vella, D.; Ajdari, A.; Vaziri, A.; Boudaoud, A. The indentation of pressurized elastic shells: from polymeric capsules to yeast cells. *J. R. Soc. Interface* **2012**, *9*, 448–55.

[S9] Pieper, G.; Rehage, H.; Barthès-Biesel, D. Deformation of a Capsule in a Spinning Drop Apparatus. *J. Colloid Interface Sci.* **1998**, *202*, 293–300.